ELSEVIER

Chemical Geology 190 (2002) 231–250

CHEMICAL GEOLOGY
INCLUDING
ISOTOPE GEOSCIENCE

www.elsevier.com/locate/chemgeo

Carbon–oxygen isotope and trace element constraints on how fluids percolate faulted limestones from the San Andreas Fault system: partitioning of fluid sources and pathways

Éric Pili[a,*], Franck Poitrasson[b], Jean-Pierre Gratier[c]

[a] *Département Analyse et Surveillance de l'Environnement, CEA/DASE/SRCE, BP 12, Bruyères-le-Châtel 91680, France*
[b] *Laboratoire de Géochimie, UMR 5563, "Mécanismes de Transfert en Géologie", CNRS-Université Paul Sabatier, 38 rue des 36 Ponts, Toulouse 31400, France*
[c] *LGIT CNRS-Observatoire-IRIGM, BP 53, Grenoble 38041, France*

This paper is dedicated to the memory of Samuel Epstein, for his remarkable work in the interdisciplinary use of stable isotope geochemistry.

Abstract

Understanding the way fluids flow in fault zones is of prime importance to develop correct models of earthquake mechanics, especially in the case of the abnormally weak San Andreas Fault (SAF) system. Because fluid flow can leave detectable signatures in rocks, geochemistry is essential to bring light on this topic. The present detailed study combines, for the first time, C–O isotope analyses with a comprehensive trace element data set to examine the geometry of fluid flow within a significant fault system hosted by a carbonate sequence, from a single locality across the Little Pine Fault–SAF system. Such a fault zone contains veins, deformation zones, and their host rocks. Stable isotope geochemistry is used to establish a relative scale of integrated fluid–rock ratios. Carbonate $\delta^{18}O$ varies between 28 ‰ and 15 ‰ and $\delta^{13}C$ between 5 ‰ and −7 ‰. From highest to lowest delta values, thus from least to most infiltrated, are the host rocks, the vein fillings, and the deformation zone fillings, respectively. Infiltration increases toward fault core. The fluids are H_2O–CO_2 mixtures. Two fluid sources, one internal and the other external, are found. The external fluid is inferred to come essentially from metamorphism of the Franciscan formation underneath. The internal (local) fluid is provided by a 30% volume reduction of the host limestones resulting from pressure solution and pore size reduction. Most trace elements, including the lanthanides, show enrichment at the 100-m scale in host carbonate rocks as fluid–rock ratios increase toward the fault core. In contrast, the same trace element concentrations are low, relative to host rocks, in veins and deformation zone carbonate fillings, and this difference in concentration increases as fluid–rock ratio increases toward the fault core. We suggest that the fluid trace elements are scavenged by complexation with organic matter in the host rocks. Elemental complexation is especially illustrated by large fractionation of Y–Ho and Nb–Ta geochemical pairs. Complexation associated with external fluid flow has a significant effect on trace element enrichment (up to 700% relative enrichment) while concentration by pressure solution associated with volume decrease of host rocks has a more limited effect (up to 40% relative enrichment). Our observations from the millimeter to the kilometer scale call for the partitioning of fluid sources and pathways, and for a mixed focused–pervasive fluid flow mechanism. The fluid mainly flows within veins and deformation zones and, simultaneously, within at least 10 cm from these channels, part of the fluid flows pervasively in the host rock, which controls the fluid composition. Scavenging of the fluid rare earth elements (REE) by host rocks is responsible for the formation of REE-depleted vein and deformation zone carbonate fillings. Fluid flow is not only

* Corresponding author. Tel.: +33-1-69-26-50-11; fax: +33-1-69-26-70-65.
E-mail address: Eric.Pili@cea.fr (É. Pili).

0009-2541/02/$ - see front matter © 2002 Elsevier Science B.V. All rights reserved.
PII: S0009-2541(02)00118-3

restricted to veins or deformation zones as commonly believed. An important part of fluid flow takes place in host rocks near fault zones. Hence, the nature of the lithologies hosting fault zones must be considered in order to take into account the role of fluids in the seismic cycle.
© 2002 Elsevier Science B.V. All rights reserved.

Keywords: San Andreas Fault; Fluids; Carbon and oxygen stable isotopes; Trace elements; REE; Y–Ho and Nb–Ta geochemical pairs; Structural geology

1. Introduction

Fluids are suspected to play a major role in earthquake mechanics and active faulting (e.g., Hickman et al., 1995; Rice, 1992; Sibson, 1994) especially in the case of the giant strike–slip system of the San Andreas Fault (SAF), California, which shows an apparent weakness (Lachenbruch and Sass, 1980). However, the origin of these fluids and the way they permeate through rocks remain poorly known. Geochemistry can help answer these questions. The nature and the origin of fluids on a vast portion of the San Andreas Fault have been documented on the basis of a comprehensive stable isotope and noble gas survey comparing fault zones and vein fillings with their host rocks and the fluids associated with these materials as sampled by fluid inclusions. These H_2O and CO_2 fluids appear to have both local, deep crustal metamorphic and mantle sources (Pili et al., 1998, in preparation). A detailed study combining structural geology, stable isotope, and rare earth elements (REE) geochemistry focused on limestones from a single locality is presented here in order to document how these fluids percolate rocks during seismic and interseismic stages.

Depending on their internal or exotic origin, and whether they come from a localized or a pervasive source, fluids may percolate pervasively through rocks or be focused into structures relatively more permeable than the bulk host, such as voids, fractures, fault planes, and gouges. Deformation is a driving force for fluid flow because it generates pressure or permeability gradients, and can lead to the generation or destruction of fluid pathways. Deformation can also be associated with production of fluid and mineral filling by means of pore size reduction and pressure solution (Gratier et al., 1993), or metamorphic reactions. Deformation can be superimposed upon the fluid–rock system, or can internally arise from the pressurized fluid inside the considered volume of host rock. Episodic fluid flow is expected to occur in and around faults in seismogenic regime, due to dilatancy and fault network connection, permeability change, and fracture sealing (Scholz, 1989; Boullier and Robert, 1992; Sibson, 1992; Robert et al., 1995). Fluid pressure changes from near hydrostatic value after an earthquake to near lithostatic value before the next earthquake. In each point where the fluid pressure overcomes the rock strength, a crack opens, and the pressure drop may lead some other fractures to close. This creates a dynamic organization of the fracture network in the rock (Jamtveit et al., 2000) driven by fluid injections. It is, thus, inferred that there is no preestablished vein network for fluid to flow in, but veins are opened at high fluid pressure when earthquake occurs and sealed once the fluid pressure drops. High fluid pressure is recovered during interseismic period (Li et al., 1998) both due to fluid flow from depth and to pressure solution crack sealing (Gratier et al., submitted for publication).

Besides structural and petrographic evidence, these fluid–rock interactions are likely to leave geochemical imprints. Through the combined used of stable carbon–oxygen isotope, trace element geochemistry, and structural analysis, the aim of this study is to highlight these imprints and to derive geochemical constraints on how fluids percolate faulted limestones in a locality along the Little Pine Fault from the San Andreas Fault system.

2. Geological setting

The San Andreas Fault system is a composite network of a high number of faults more or less active since 30 Ma, predominantly accommodating the relative motion between the North American and Pacific plates as a strike–slip system (e.g., Wallace, 1990). Several major sets of faults, such as the Santa Ynez, the San Andreas *s.s.*, and the San Gabriel

faults subsystems compose the SAF system from San Francisco to Los Angeles (see Fig. 1). The Santa Ynez fault subsystem is a former strand of the San Andreas Fault formed in the early development of the fault system and rotated. Numerous short length faults (<60 km) developed adjacent to the major ones and ultimately merged with them, such as the Little Pine Fault in the Santa Ynez subsystem (Fig. 1). The Little Pine Fault is a thrust fault with a length of 55 km. It is hosted by the Miocene Monterey Formation (hemipelagic, organic-rich carbonate sediments) and the Cretaceous Franciscan Formation (graywackes and serpentinites) underneath. More details about the local geology are given in Dibblee (1966). The Little Pine Fault dips to the northeast. Its most recent rupture is Late Quaternary to Prequaternary (Jennings, 1994).

Our studied site (approximately W 119°40′, N 34°32′) crops out over 500 m across the Little Pine Fault, East of Lake Cachuma, Santa Ynez Mountains. In the field, the fault is defined by a main damaged zone ca. 3 m wide, and several secondary adjacent damaged zones with various spacing and decreasing width away from the fault core. The damaged zones are made of gouges, fault planes, fault veins, and extension veins (see below). Fault planes, fault veins, and gouges are altogether hereafter referred to as deformation zones by contrast with veins (extension fractures sealed) and host rocks. Gouges are a mechanical mixture of broken host rocks, new mineral phases precipitated from interacting fluids, and recrystallized host rock minerals. Gouges range from breccias to cataclasites or mylonites. Fault planes are narrow zones of shearing that frequently expose polished surfaces with slickenside structures. As a fault plane is approached, the host rock is increasingly brecciated; particle size (rock pieces or minerals) decreases, and the amount of reworked material increases with increasing amount of mass transfer as shown by calcite precipitates. Fault veins also developed parallel to fault planes by sealing of the fault opening and present slickenside structures.

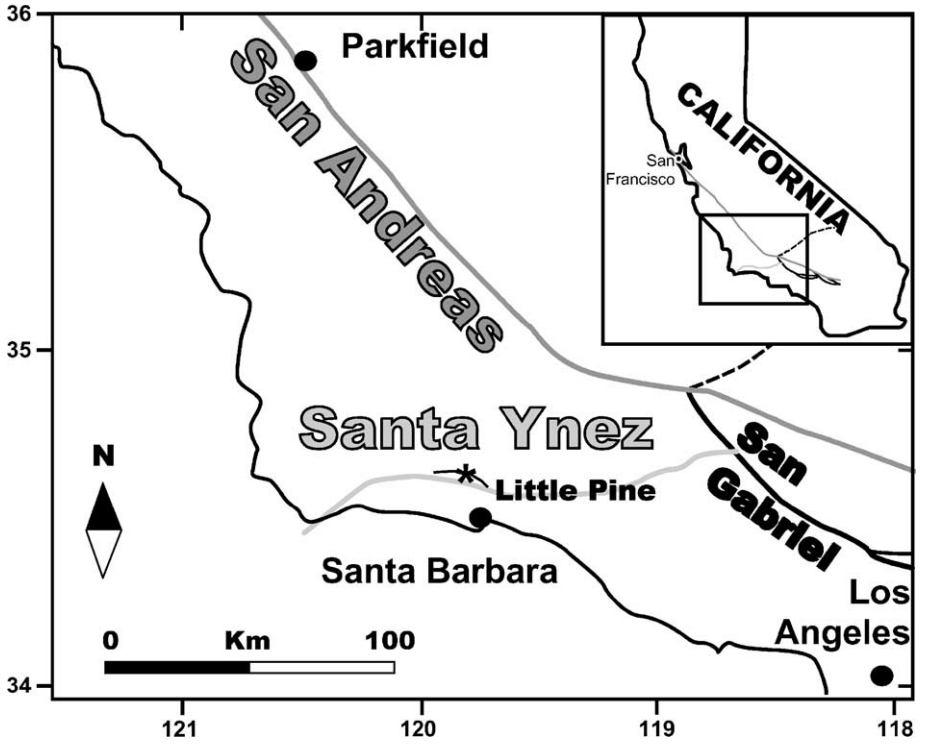

Fig. 1. Location of the Little Pine Fault and the sample locality (star) within the San Andreas Fault system. The three major sets of faults are indicated: Santa Ynez, San Andreas (strictly speaking), and San Gabriel faults. Filled circles are reference localities.

Table 1
Carbonate[a] isotope compositions from deformation zones, veins, and their host rocks

Sample	Sample type (from field and thin section)	Distance (m) from fault core	Setting[b]	$\delta^{18}O$ (‰, SMOW)	$\delta^{13}C$ (‰, PDB)
LP2 H	sheared graywacke	0	DZ	27.33	− 7.15
LP2 V	calcite vein	0	V	22.61	− 5.09
LP4 H	host limestone	3	H	22.59	− 1.31
LP4 V	1-mm vein		V	21.51	− 1.61
LP4 C	carbonate breccia clasts		DZ	19.61	− 6.72
LP4 M	limestone gouge		DZ	19.78	− 7.05
LP5 H	host limestone	7	H	22.74	− 3.80
LP5 V	5-mm-wide vein		V	21.22	− 1.60
LP7 H	host limestone	10.5	H	23.37	1.97
LP7 V-Cc	calcite from 35-mm-wide vein		V	24.02	0.67
LP7 V-Dolo	dolomite from 35-mm-wide vein		V	24.21	− 2.28
LP7 V-totCarb	total vein carbonate[c]		V	24.04	0.47
LP8 H	host limestone	12.5	H	25.15	2.67
LP8 V	3-mm-wide vein		V	23.01	2.15
LP9 H	host limestone	12.7	H	25.89	− 0.66
LP9 V	10-mm-wide vein		V	20.31	− 3.78
LP10 H	host limestone	16	H	20.96	− 3.44
LP10 V	100-mm-wide vein		V	16.96	− 3.62
LP11aH	host limestone	22.5	H	23.22	− 0.07
LP11a V	3-mm-wide vein		V	19.63	− 0.42
LP11b H	host limestone	22.5	H	24.40	0.15
LP11b V.I	1-mm-wide vein, stage 1		V	21.52	− 0.31
LP11b V.II	3-mm-wide vein, stage 2		V	19.55	− 0.77
LP11b V.III	30-mm-wide vein, stage 3		V	19.74	− 0.51
LP11c H-Cc	host limestone calcite	22.5	H	24.65	1.29
LP11c H-Dolo	host limestone dolomite		H	25.78	2.39
LP11c H-totCarb	total limestone carbonate		H	24.73	1.36
LP11c V1	early, layer-parallel, 17-mm-wide vein		V	19.63	− 0.72
LP11c V2	late-stage, high-angle vein		V	15.09	− 0.72
LP12 H	highly veined host limestone	50	H	22.65	− 5.43
LP12 VW	external part of 40-mm-wide vein, white		V	21.51	− 2.74
LP12 VB	9-mm-wide central part of vein, brownish		V	24.15	− 6.25
LP13 MFB1-H	host limestone	54	H	23.62	− 3.87
LP13 MFB2-M	fault plane		DZ	20.21	− 6.90
LP13 GWR	gouge		DZ	19.97	− 7.43
LP14 H	host limestone	58	H	24.44	0.47
LP14 VM	5-mm-wide fault vein with slickensides		DZ	16.17	− 4.14
LP15 H	host limestone	64	H	25.77	3.23
LP15 V	2-mm-wide vein		V	15.51	− 4.85
LP16 H	host limestone	71	H	27.96	7.31
LP16 V	vein		V	25.39	4.28
LP16 M	fault plane, slickensides		DZ	22.36	− 3.18
LP16 M2	fault plane, slickensides		DZ	21.29	− 2.03
LP17 V	vein	85	V	17.25	− 7.09
LP18 H	host limestone	125	H	25.56	3.21
LP18 V	vein		V	23.48	− 0.68
LP19 H	host limestone	500	H	27.16	5.26
LP19 V	vein		V	21.56	− 3.08
LP19 M	fault plane		DZ	18.32	− 4.32

[a] Carbonate is calcite unless otherwise stated.
[b] DZ = deformation zone; V = vein; H = host rock.
[c] Total carbonate composition calculated from calcite and dolomite compositions and abundances.

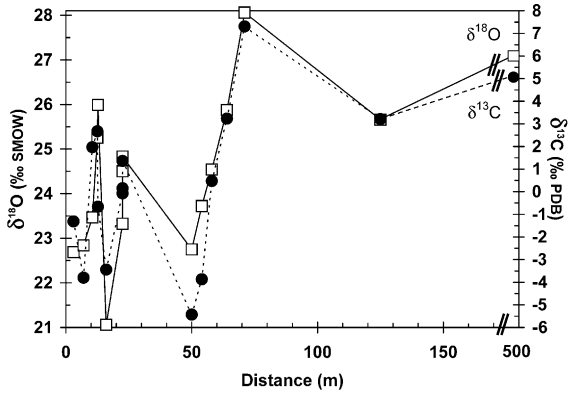

Fig. 2. Variations of $\delta^{13}C$ (black circles) and $\delta^{18}O$ (white squares) in host limestone carbonates as a function of distance from Little Pine Fault core. Note the gap in the distance axis for the last sample that is located 500 m away from fault core. C and O isotope compositions remarkably follow the same variations except for the first sample (closest to fault core). Large decreases in isotopic ratios in host rock coincide with the occurrence of highly deformed (and infiltrated, see text) zones: repeated fault planes, large veins, and local high density of veins.

Veins anastomose as their number increases toward the fault core. Successive episodes of fracturation are revealed by cross-cutting vein generations. Typical vein spacing decreases from more than 5 to 10 cm along a 200-m profile toward the fault core. This indicates an increasing bulk permeability toward the fault core. Veins developed as fractures during earthquakes or during the related interseismic deformation since their orientations are kinematically consistent with neighboring fault displacements.

We systematically sampled deformation zones, veins, and host rocks over a 500-m-long section across the Little Pine Fault. We collected over 40 samples. In each hand specimen, the host rock is sampled within 1–10 cm from the associated vein and deformation zone. It is difficult to find unaltered host rocks—devoid of fluid infiltration effects related to the Little Pine Fault, but nevertheless representative of the original chemistry of the rocks before faulting—that can be used as a chemical and isotopic reference. We assume negligible lateral chemical heterogeneity of the Monterey limestones over 500 m and took our reference sample 500 m away from the fault core, although it is still possible to find veins or deformation zones at this distance. Sample description is presented in Table 1.

3. Stable isotopes: analytical methods and results

Carbon and oxygen isotope analyses are reported with the δ notation in per mil with reference to PDB and SMOW standards, respectively. Isotopic compositions and yields for carbonate were measured on CO_2 gas extracted via H_3PO_4 (McCrea, 1950), on an automated carousel for calcite-rich samples (12 min at 90 °C) and manually for mixed calcite–dolomite samples (extractions after 1 and 5 days of reaction). However, as dolomite content was <6%, isotope measurements

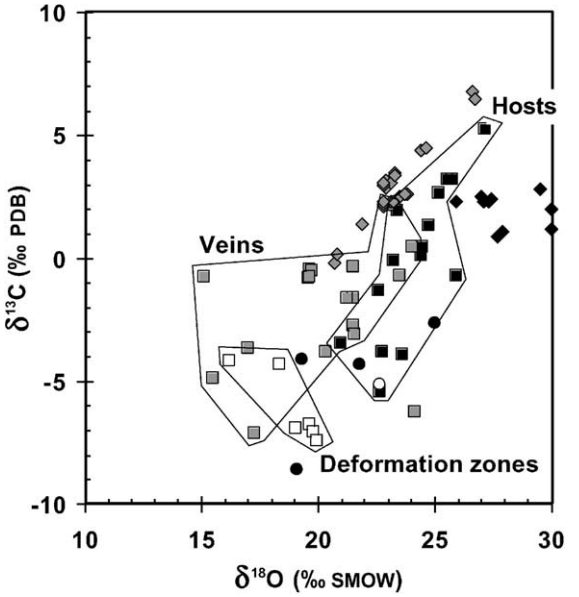

Fig. 3. Carbon and oxygen isotope compositions of carbonates from host limestones (solid squares), veins (shaded squares), and deformation zones (open squares) taken across the Little Pine Fault. One point corresponding to a late vein filling (sample LP12 VB; see Table 1) has been omitted from the field drawn for the vein isotopic compositions. Large isotope shifts with more or less correlated C–O isotope values imply infiltration by external mixed H_2O–CO_2 fluids. With decreasing delta values, thus with increasing integrated fluid/rock ratios (see Discussion), are the host rocks, the veins, and the deformation zones, respectively. Comparison with the compositions of diagenetic calcite veins (shaded diamonds) and their host limestones (solid diamonds) from the same Monterey Formation away from the Little Pine Fault (see Discussion); data after Winter and Knauth (1992). The composition of a calcite vein hosted in graywackes within the fault core (open circle) plots as end-member for the fluid infiltrated in the host limestones of the Little Pine Fault. So do calcite compositions from various Franciscan carbonated host rocks (solid circles); data after Magaritz and Taylor (1976).

from automated carousel extractions and manual extractions (after bulk carbonate content recalculation) agreed to within 0.2‰. Analytical precision was ±0.05‰ for carbon and ±0.1‰ for oxygen. The carbon and oxygen isotope compositions of carbonates from host rocks, veins, and deformation zones are presented in Table 1 and in Figs. 2 and 3. Since carbonates are main minerals of limestones, comparison of isotope compositions of veins, deformation zones, and host rocks can be made on samples having the same mineralogy. In addition, carbonate analyses lead to two isotopic compositions ($\delta^{13}C$ and $\delta^{18}O$), which are of great help when deciphering H_2O-CO_2 fluid–rock interactions.

Details in the variation of $\delta^{13}C$ and $\delta^{18}O$ values in host limestone with distance from the fault core are presented in Fig. 2. The C and O isotope compositions show the same trends except for the sample closest to fault core. A lowering of the isotopic ratios coincides with the occurrence of highly deformed zones: repeated fault planes, large veins, or local high density of veins. The $\delta^{13}C$ vs. $\delta^{18}O$ diagram (Fig. 3) shows the consistent variations of these two isotopic compositions in host rocks. The host rock limestones

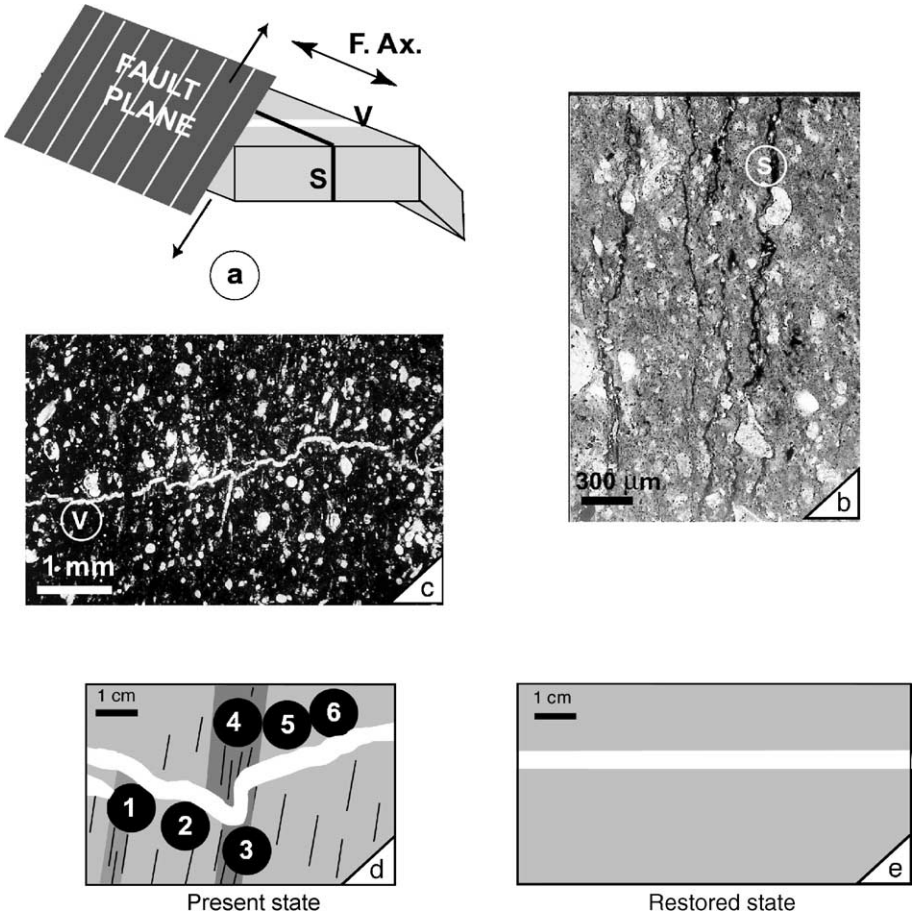

Fig. 4. Setting of pressure solution and crack sealing across the Little Pine Fault. (a) Schematic view of the structural setting at the scale of the outcrop (10–100 m), with indication of the fault plane, fold axis (F.Ax.), cleavage (S), and veins (sealed fractures, V). (b) Pressure solution cleavage (S) in thin section. (c) Thin section of an early filled fracture (V) folded during progressive deformation. (d) Schematic view of the development of tectonic layering related to pressure solution in rock matrix near folded veins, observed about 10 m from the fault core, with the location of the most deformed samples (P1, P3, P4) near the limb of the folded veins and the least deformed samples (P2, P5, P6) near the horizontal part of the folded veins. (e) Restoration of the deformed strata shown in (d).

show a large carbon and oxygen isotope range, with 21‰ $<\delta^{18}O<$ 28‰ (average 24.3 ± 1.8‰, 1σ) and −5‰ $<\delta^{13}C<$ 5‰ (average 0.4 ± 3.5‰). Veins have distinct compositions lower by up to 8‰ for carbon and up to 10‰ for oxygen with respect to their host rocks, with 15‰ $<\delta^{18}O<$ 25‰ (average 20.6 ± 2.9‰) and −7‰ $<\delta^{13}C<$ 2‰ (average −1.7 ± 2.7‰). Successive vein generations show lower delta values with time, as illustrated by sample series LP11b and LP11c (see Table 1). Deformation zones show low and less variable delta values, with 16‰ $<\delta^{18}O<$ 22‰ (average 19.7 ± 1.9‰) and −7‰ $<\delta^{13}C<$ −4‰ (average −5.2 ± 2.1‰). They exhibit distinctly lower isotopic ratios with differences up to 9‰ for carbon and oxygen compared to their host rock. Decreasing isotopic ratios are even observed in a single hand specimen for carbonate from host rocks, veins, and deformation zones, respectively, as shown in sample series LP4, LP16 and LP19 (see Table 1).

4. Major and trace elements: analytical methods and results

Two subsample sets were chosen for trace elements analyses. One is composed of six samples collected along a centimeter scale profile from a single tectonized strata 10 m away from fault core (sample series P1–P6) and is used to compare the behaviors of trace (Table 3) and major (Table 4) elements during deformation of the host rock (see Fig. 4). The other sample

Table 2
Trace elements concentrations (ppm) and ratios in host limestones, veins, and deformation zones

Sample	LP9 H	LP9 V	LP14 H	LP14 VM	LP19 H	LP19 V	LP19 M
Sample type	Host	Vein	Host	Fault plane	Host	Vein	Fault plane
Distance from fault core (m)	13	13	58	58	500	500	500
Ba	135	17.7	169	24.0	263	26.9	22.1
Pb	8.92	3.04	17.9	1.18	28.3	5.93	6.16
Sr	546	201	823	399	606	578	1140
La	7.87	1.89	4.42	0.067	1.20	0.719	0.324
Ce	11.2	1.64	5.86	0.144	1.39	0.688	0.267
Pr	1.56	0.179	0.858	0.020	0.223	0.105	0.037
Nd	6.51	0.641	3.48	0.075	0.897	0.436	0.132
Sm	1.296	0.092	0.715	0.02	0.185	0.073	0.035
Eu	0.334	0.034	0.149	0.005	0.052	0.017	0.009
Gd	1.52	0.171	0.745	0.011	0.204	0.099	0.035
Tb	0.236	0.031	0.117	<0.0006[a]	0.027	0.014	0.008
Dy	1.61	0.250	0.791	0.017	0.183	0.112	0.037
Y	14.1	4.37	8.14	0.212	1.81	1.34	0.622
Ho	0.368	0.073	0.182	0.003	0.042	0.027	0.010
Er	1.10	0.261	0.558	0.015	0.125	0.083	0.034
Tm	0.153	0.039	0.075	0.001	0.018	0.011	0.006
Yb	0.969	0.259	0.465	0.012	0.111	0.080	0.045
Lu	0.152	0.041	0.071	0.002	0.017	0.012	0.007
Th	1.59	0.015	0.813	0.018	0.167	0.042	0.006
Zr	37.2	0.372	20.7	0.466	5.52	1.60	0.826
Hf	1.06	<0.001[a]	0.478	<0.001[a]	0.091	0.009	<0.001[a]
Nb	1.84	0.024	1.39	0.041	0.273	0.066	0.006
Ta	0.745	0.800	0.522	0.651	0.498	0.290	0.405
U	14.9	1.80	3.13	0.075	0.573	0.267	0.057
Y/Ho	38.2	59.7	44.7	63.8	43.4	49.8	64.6
Zr/Hf	35.0	n.c.	43.7	n.c.	60.4	170	n.c.
Nb/Ta	2.47	0.03	2.66	0.06	0.55	0.23	0.01
$\delta^{13}C$[b]	−0.66	−3.78	0.47	−4.14	5.26	−3.08	−4.32
$\delta^{18}O$[b]	25.89	20.31	24.44	16.17	27.16	21.56	18.32

[a] This value is the detection limit. n.c.: not calculated.
[b] Data from Table 1, in per mil.

set is composed of three hand specimens chosen in the light of the stable isotope results for the LP sample series. This set is used to document the relative variations of trace element contents between veins and/or deformation zones and their host rocks, and between host rocks, as a function of distance from fault core. It is subdivided as follows (see Table 2): one vein and its host located 13 m from fault core (respectively, samples LP9 V and LP9 H); one fault plane and its host located 58 m from fault core (respectively, samples LP14 VM and LP14 H); one fault plane, one vein, and their host rock located 500 m from fault core (respectively, samples LP19 M, LP19 V and LP19 H).

Major elements of the P sample series (Table 4) were analyzed at CNRS-CRPG (Nancy, France) with a JY70 ICP-AES after lithium metaborate fusion and acid decomposition. Given the sample concentrations (Table 4), the uncertainties may vary from better than 1% for SiO_2 and CaO to up to 10% (relative standard deviation) for the other elements.

Trace element analyses of the LP sample series (Table 2) were carried out at CNRS-LMTG (Toulouse, France). One hundred milligrams of powdered rock was mixed with 320 mg of $LiBO_2$ and 80 mg of $Li_2B_4O_7$. The mixture was then fused in a platinum crucible using a Mecker burner at ca. 1000 °C for 15 min. After cooling, the resulting bead was dissolved in 4% HNO_3 on a hot plate. The sample was diluted with Milli-Q water and bidistilled HNO_3, and In and Re were added as internal standards to about 10 ppb in the final 2% HNO_3 solution. This results in an overall sample dilution factor of about 3000 by weight. About 30 trace elements were analyzed with an Elan 6000 ICP-MS calibrated using commercial standard solutions. Uncertainties are better than 10% (relative standard deviation), as estimated from rock standard analyses for concentrations down to 0.3 ppm. Below that value, uncertainties may reach 15%.

Trace elements of the P sample series (Table 3) were analyzed at CNRS-CRPG with an Elan 5000 ICP-MS after lithium metaborate fusion and acid decomposition. Uncertainties are better than 10% (relative standard deviation), as estimated from rock standard analyses, except for Pb for which uncertainties may reach 20%. Details on procedures may be found in Carignan et al. (2001).

Table 3
Trace element concentrations (ppm) in six samples from one deformed strata[a]

	Least deformed samples			Most deformed samples		
	P6	P5	P2	P1	P4	P3
Ba	117	145	125	187	132	127
Pb	2.88	3.34	4.34	4.69	7.66	6.95
Rb	6.32	7.57	6.79	11.2	7.9	7.48
Sr	710	708	622	660	599	630
La	4.83	5.72	5.95	10.2	6.52	6.55
Ce	7.13	9.31	9.73	17.7	11.4	11.5
Pr	0.905	1.2	1.2	2.16	1.39	1.43
Nd	3.49	4.56	4.67	7.74	5.37	5.17
Sm	0.704	0.891	0.893	1.63	1.14	1.03
Eu	0.174	0.175	0.177	0.352	0.207	0.208
Gd	0.705	0.918	0.86	1.37	0.992	1.05
Tb	0.101	0.149	0.129	0.229	0.151	0.183
Dy	0.73	0.852	0.83	1.39	1.01	1.08
Y	7.18	7.62	6.59	8.75	7.78	7.68
Ho	0.174	0.194	0.203	0.306	0.228	0.257
Er	0.404	0.514	0.55	0.768	0.597	0.704
Tm	0.069	0.085	0.088	0.123	0.087	0.104
Yb	0.436	0.505	0.551	0.765	0.579	0.711
Lu	0.073	0.073	0.086	0.113	0.088	0.106
Th	0.82	1.69	2.77	3.15	4.05	4.65
Zr	20	25.7	25.8	46.5	27.3	28.7
Hf	0.52	0.69	0.84	1.4	0.84	0.95
Nb	0.97	1.22	1.23	2.11	1.46	1.61
Ta	0.1	0.15	0.22	0.28	0.25	0.27
U	4.66	5.54	6.65	7.04	6.84	6.4
Y/Ho	41.3	39.3	32.5	28.6	34.1	29.9
Zr/Hf	38.5	37.2	30.7	33.2	32.5	30.2
Nb/Ta	9.7	8.1	5.6	7.5	5.8	6.0

[a] See Fig. 4 for sample locations.

The trace element contents of the various rock types (Tables 2 and 3) vary by a factor of 150, although their lanthanide distribution appears to be broadly similar, and shows subparallel patterns (Fig. 5). Rare earth concentrations tend to decrease from the host rocks to the veins, and to the deformation zones. Within a single host rock hand specimen, samples from the most deformed zone (P1, P3, P4; see Fig. 4d and Table 3) tend to show higher trace element concentrations than samples from the least deformed zone (P2, P5, P6). Lanthanide concentrations in the host limestones increase toward the fault core (compare samples LP19 H, LP14 H, and LP9 H in Fig. 5).

Like lanthanides, the trace element patterns from three host limestones (Fig. 6) show enrichments toward the fault core for all the measured trace elements, except for Ba and Pb that are depleted,

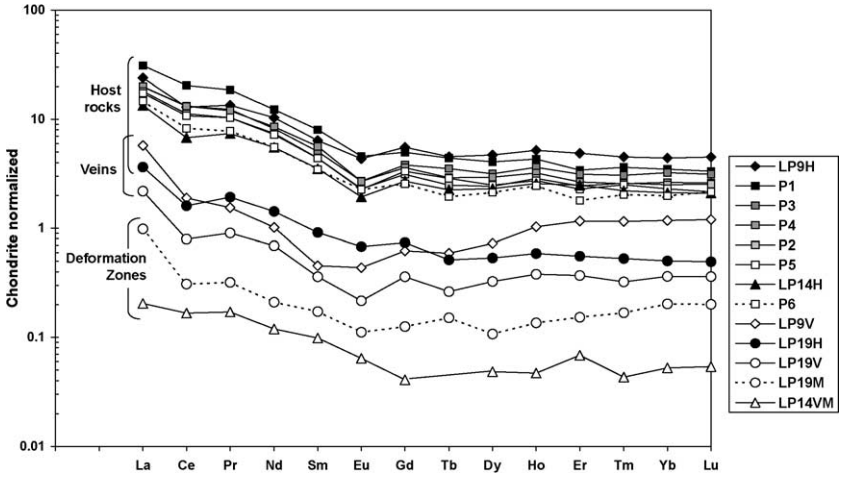

Fig. 5. Plot of the REE concentrations for all the analyzed samples, subdivided into host rocks, veins, and deformation zones. Data are from Tables 2 and 3. Chondrite normalization values after Nakamura (1974). The REE patterns are subparallel; the seawater Ce anomaly is preserved (see text). Lanthanide concentrations tend to decrease from the host rocks to the veins, then to the deformation zones. By contrast, within a single host rock hand specimen, samples from the most deformed zone (P1, P3, P4) tend to have higher trace element concentrations than the least deformed zone (P2, P5, P6). Similarly, REE concentrations are higher in the host limestones (LP9 H, LP14 H) sampled within 60 m from fault core than in the host limestone 500 m away (sample LP19 H).

and Sr and Ta that are nearly constant. For samples LP9 H (13 m from fault core) and LP14 H (58 m from fault core), enrichments in REE show a mean factor of ca. 8 (+700%) and 4 (+300%), respectively, compared to the least altered host limestone (LP19 H, 500 m from fault core).

The trace element patterns in deformation zones and veins are depleted compared to their host rocks (see Fig. 7), except for two deformation zones where Sr is enriched in sample LP19 M and Ta is enriched in sample LP14 VM. At a given distance from fault core, REE depletion is higher in deformation zones than in

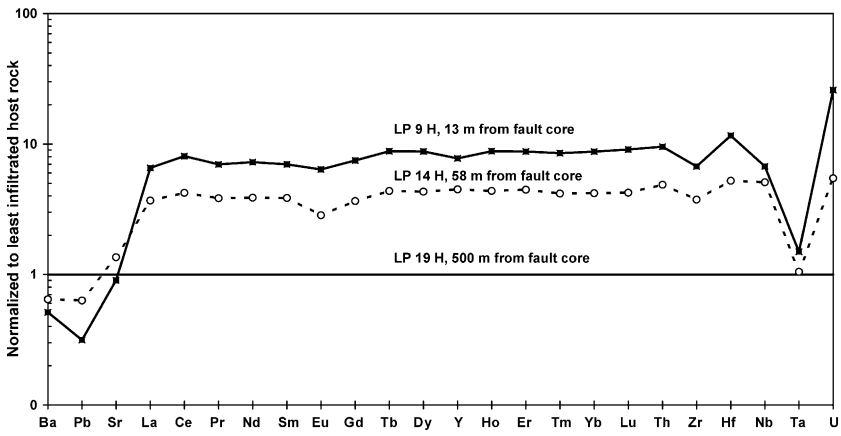

Fig. 6. Trace element concentrations in host limestones from three sampling points across the Little Pine Fault. Concentrations are normalized to those from the remote, least infiltrated, sample 500 m away from fault core (LP19 H). Most trace elements, notably all the REE, are enriched in host rocks as fluid–rock ratios increase toward the fault core (see text and Fig. 3). Trace elements are sorted from left to right with increasing ionic charge and decreasing ionic radius. Data are from Table 2.

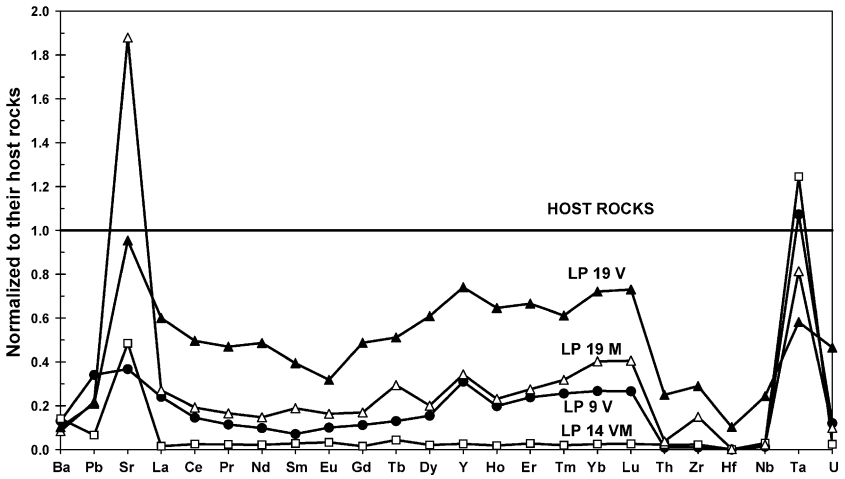

Fig. 7. Trace element concentrations normalized to their host rocks for veins and deformation zones from three sampling points across the Little Pine Fault. Most of trace elements, including all the REE, are depleted in veins and deformation zones as fluid–rock ratios increase toward the fault core (see text and Fig. 3). Data are from Table 2.

veins, and shows a mean factor of ca. 0.02 (− 98%) and 0.25 (− 75%) in the deformation zones compared to their host rocks, for samples LP14 VM (58 m from fault core) and LP19 M (500 m from fault core), respectively. Depletion in REE show a mean factor of ca. 0.2 (− 80%) and 0.6 (− 40%) in the veins compared to their host rocks, for samples LP9 V (13 m from fault core) and LP19 V (500 m from fault core), respectively. Thus, REE are increasingly depleted in veins and deformation zones toward the fault core (Fig. 7) while they are increasingly enriched in host rocks (Fig. 6).

5. Pressure solution, fluid production, and crack sealing

Pressure solution in the faulted Monterey Formation is an important deformation mechanism. Vertical solution cleavage, parallel to the axial plane of folds (several tens of meters in size), is found up to several tens of meters from the fault (Fig. 4a). Fold axes and cleavage (Fig. 4b) are subparallel to the fault direction, reflecting intense shortening more or less perpendicular to this fault direction, thus indicating that these deformations are related to thrust displacement. Tension gashes are vertical and perpendicular to solution cleavage in near horizontal strata. Younger veins are almost undeformed with planar walls, whereas earlier veins were developed and then folded during the progressive deformation of the rocks (Fig. 4c). The shortening perpendicular to the cleavage is estimated by unfolding the earliest veins (Fig. 4d and e). This gives a minimum mean value of − 30% over tens of meters along the outcrop. The elongation that simultaneously occurred in the direction perpendicular to the vein can be estimated by summing the widths of

Table 4
Major element concentrations (wt.%) in six samples from one deformed strata[a]

	Least deformed samples			Most deformed samples		
	P2	P5	P6	P1	P3	P4
SiO_2	29.1	33.2	28.5	26.4	26.9	31.4
Al_2O_3	2.05	1.9	1.58	2.18	2.71	2.55
Fe_2O_3	0.65	0.68	0.61	0.83	0.88	0.88
MnO	< 0.03[b]	< 0.03[b]	< 0.03[b]	0.03[b]	< 0.03[b]	0.33
MgO	1.09	0.88	0.95	1.17	1.24	1.16
CaO	35.8	33.5	36.2	36.3	35.6	33.1
Na_2O	< 0.05[b]	< 0.05[b]	< 0.05[b]	< 0.05[b]	< 0.05[b]	< 0.05[b]
K_2O	0.15	0.15	0.12	0.17	0.18	0.18
TiO_2	0.06	0.06	0.05	0.07	0.08	0.08
P_2O_5	0.19	0.22	0.2	0.25	0.25	0.24
Loss on ignition	31.1	29.2	31.5	32.4	31.9	30.1
Total (%)	99.8	99.8	99.8	99.8	99.8	100.1

[a] See Fig. 4 for sample locations.
[b] This value is the detection limit.

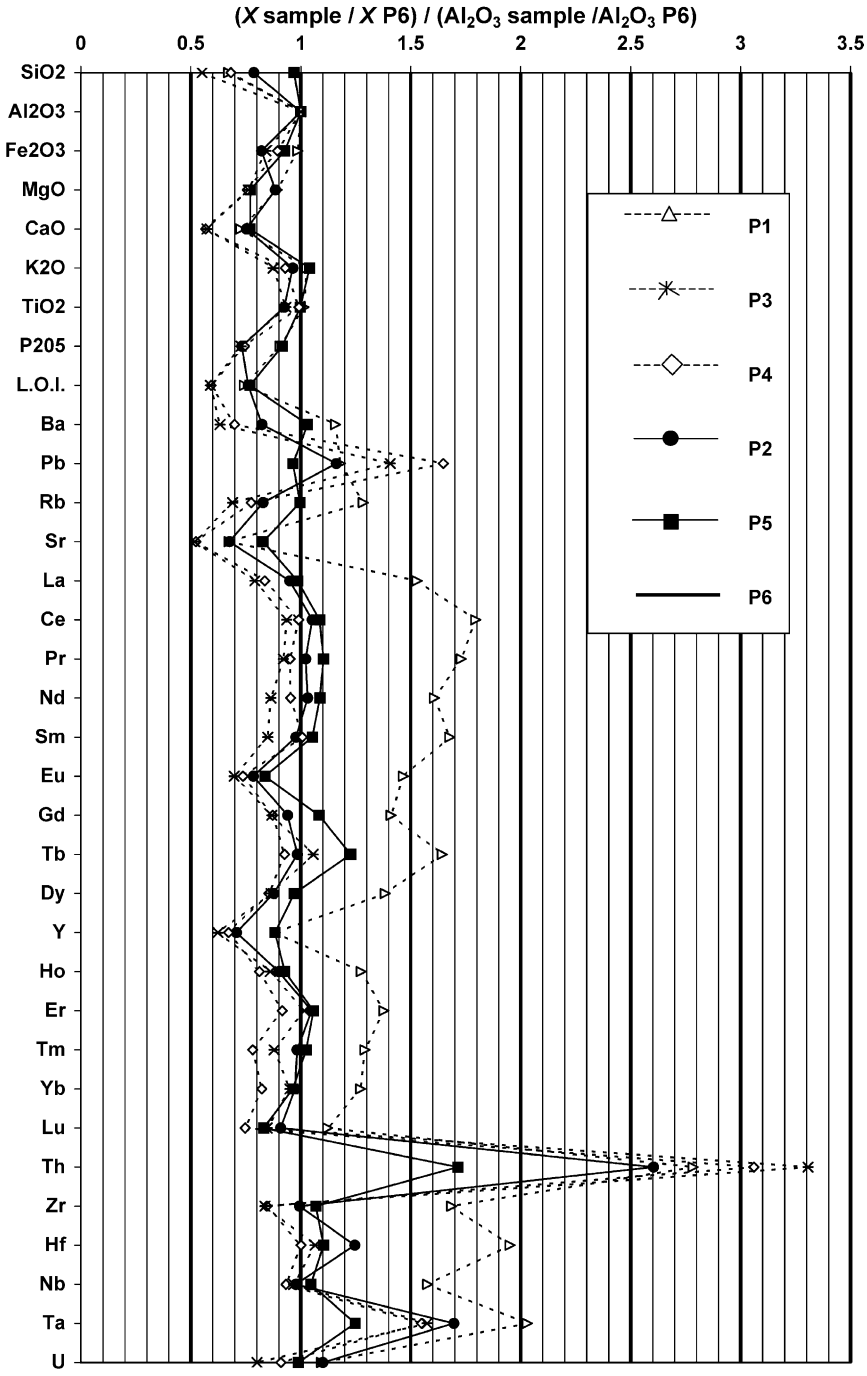

Fig. 8. Major and trace element concentrations in variously deformed host rock samples from a centimeter scale profile normalized to the least deformed one (sample P6) and to the Al_2O_3 content. See Fig. 4 for structural setting. Data are from Tables 3 and 4. The more deformed samples (P1, P3, P4) show higher depletions/enrichments than the less deformed ones (P2, P5, P6). Dissolution of quartz, calcite, and dolomite (Si, Ca, and Mg) leads to passive concentration of kaolinite and oxide minerals (Al, Fe, Ti). Most of the trace elements, including all the REE but Eu, follow the passive concentration of the major elements that are not involved in the dissolution process. Other trace elements (Ba, Rb, Sr, Y) follow the behavior of the major elements remobilized and are depleted because of host mineral dissolution.

each vein at the same scale and is found to be only 1–2%. This geometrical analysis indicates a significant decrease in rock volume (-30%) associated with pressure solution.

The effects of this deformation process on the mobility of the major and trace elements can be estimated by comparing chemical analyses, when insoluble species are passively concentrated by the dissolution of soluble species (Gratier, 1983). The P sample series has been collected for this purpose along a centimeter scale profile in a given tectonized strata (Fig. 4d) about 10 m from the fault core. We compared trace (Table 3) and major (Table 4) element concentrations of the most deformed host rock samples (P1, P3, P4) with the less deformed ones (P2, P5, P6). Fig. 8 presents these concentrations normalized to those of an assumed insoluble major element (Al) from the least deformed sample (sample P6). The more deformed samples show higher depletions/enrichments than the less deformed ones. Major elements show that dissolution of quartz, calcite, and dolomite (see elements Si, Ca, and Mg, with concentration ratios significantly lower than 1 in Fig. 8), leading to passive concentration of kaolinite and oxide minerals (Al, Fe, Ti, with concentration ratios close to 1), is associated with deformation at the millimeter to decimeter scales. In Fig. 8, most of the trace elements, including all the REE but Eu, follow the passive concentration of some of the major elements, with concentration ratios between 0.75 and 1.20—thus not significantly different from 1—with the uncertainties on the calculated ratios being less or equal to $\pm 20\%$. Eu is depleted. Except for sample P1 (taken next to a partially dissolved fossil) that shows significant enrichment of all the REE, very few elements (Pb, Th, Ta) show an enriched concentration, predominantly in the most deformed sectors. Other trace elements (Ba, Rb, Sr, Y) follow the behavior of the major elements remobilized and are depleted because of host mineral dissolution, with concentration ratios as low as 0.5. Thus, the behavior of the major and compatible trace elements is consistent with the global volume decrease of the deformed host rocks. Mass transfer balance at the tectonic layer scale implies that the local amount of dissolution is much greater than the amount of precipitation. Consequently, part of the soluble species removed by dissolution along the solution cleavages and subsequent rock volume reduction has been expelled with fluid from the host rocks and may have contributed to sealing the veins nearby. This is the internal fluid production process. Our comparative chemical analysis combined with the global volume decrease of ca. -30% of the deformed host rocks indicates that the fluid expelled from the deformed host rocks can be enriched in REE by up to 40%.

6. Discussion

6.1. Fluid nature and sources

The closely related carbon and oxygen isotope variations in carbonate host rocks (Figs. 2 and 3) imply infiltration of fluids containing both carbon and oxygen, such as CO_2-rich ones. In contrast, the rather decoupled C and O isotope variations observed for veins and deformation zones compared to their host rocks (Fig. 3), and particularly the occurrence of large O isotope shift with nearly constant C isotope compositions (see in Table 1 samples LP8 H and V, LP10 H and V, LP11a H and V, and LP11b H and V), imply that another type of fluid with oxygen and very little, if any, carbon is involved, such as H_2O. The trace element behavior is also in favor of the onset of an aqueous fluid (see below). Although the trends for host rocks and veins C–O isotope compositions follow similar vectors (Fig. 3) for some veins, indicating infiltration by fluids with similar CO_2–H_2O ratios, the trends for the isotope composition of other veins, with vectors up to the horizontal, imply infiltration by fluids significantly richer in H_2O.

Two fluid sources, one internal the other external, are here evidenced from the stable isotope and trace element constraints. The carbonate mineralizations and the large isotope shifts between veins or deformation zones and their host rocks (Fig. 3) imply fluid infiltration associated with faulting, with at least part of this fluid being of exotic origin. An internal local fluid is also provided by the volume reduction of the host limestones (Figs. 4d and 8).

The trace element content of the various rock types appears to be broadly similar (Tables 2 and 3), as illustrated by REE patterns (Fig. 5). Specifically, it appears that the Ce-negative anomaly, typical of seawater and thus of carbonates that precipitated in the

marine environment (Fleet, 1984; Liu et al., 1988), is still apparent in the veins and the deformation zones. Although a strict demonstration can only be made on the basis of Nd isotopes (Poitrasson et al., 1995, 1998), all these suggest that the trace elements present in these samples bear negligible, if any, exotic components from surrounding magmatic or detrital rocks brought by the fluids associated with the main fault. Hence, the fluids responsible for the precipitation of carbonates in veins and deformation zones have their trace element geochemistry dominated by a marine carbonate source, the most likely being the Monterey Formation. The initial REE contents of the fluids flowing into the faulted Monterey Formation are therefore found to be controlled by the carbonate sequence itself. By using the appropriate distribution coefficients of REE between fluids and carbonate minerals, beyond the scope of this study, the initial REE contents of the fluids that permeate the limestones could be bracketed by the composition of our reference sample LP19 taken at 500 m from fault core, for which the REE contents of the vein and the associated host rock are close to within a factor of 3 (see Fig. 5 and Table 2). From this initial value, the REE content of the fluids increases during and after faulting due to interactions with the host rocks and the porosity reduction and pressure solution crack sealing process. However, the increase in REE concentration associated with the host rock volume reduction is modest (+40%). This shows that the deformation of the host rock cannot be the main mechanism for REE enrichment of the host rocks. Thus, the host rock REE enrichment must result from percolation of the carbonate host rocks by external fluids flowing in veins and deformation zones.

The internal fluid is difficult to characterize isotopically. The composition of a former sedimentary fluid trapped within the sediment or evolved from the sediment during diagenesis (basinal fluid) can be estimated from those of identified diagenetic calcite veins (Fig. 3, shaded diamonds) taken in the same Monterey Formation away from the Little Pine Fault (Winter and Knauth, 1992), with the host rock calcites (solid diamonds) having similar compositions in both localities. The host rock calcites sampled in the Monterey Formation away from the Little Pine Fault have $\delta^{13}C>0$ and $\delta^{18}O$ >25‰, consistent with isotopic compositions of pristine carbonated sediments and with the less altered host rock compositions measured at Little Pine away from the fault core (see Fig. 2). If the internal fluid is a former sedimentary fluid, its distinctive isotopic composition cannot be retrieved in any vein filling at Little Pine. This is explained by the pervasive flow through the host limestone porosity of the internal fluid that is expelled by the 30% volume reduction. Indeed, the slightly lower $\delta^{18}O$ values observed for the Little Pine host limestones compared to the other Monterey limestones (Fig. 3), and the isotopic evolutions of the Little Pine host limestones and the diagenetic veins along similar vectors, could result from pervasive internal fluid flow. However, this internal fluid migration cannot account for the total observed isotopic variations of the host rocks. This, again, calls for external fluid flow.

Stable isotopes show that the external fluid comes principally from metamorphism of the underlying formations. The closest underneath formation is the Franciscan melange composed of graywackes, metabasites, and metamorphozed limestones. As illustrated in Fig. 3, the composition of a calcite vein hosted in graywackes within the fault core (open circle) plots as an end-member for the fluid infiltrated in the Little Pine Fault host limestones. So do calcite compositions from various carbonated host rocks (solid circles) sampled elsewhere in the Franciscan Formation (Magaritz and Taylor, 1976). Metamorphic fluids coming from below into fault zones have also been evidenced in several locations along the SAF system from San Francisco to Los Angeles (Pili et al., 1998, in preparation). The onset in fault zones of metamorphic fluids contributed by the underlying Franciscan Formation has also been evidenced by Irwin and Barnes (1975) from their study of the chemistry of spring waters along the SAF. O'Neil and Hanks (1980) also suggested that metamorphic water from adjacent Franciscan rocks may have migrated into the SAF system. Eichhubl and Boles (2000) evidenced that the upward cross-stratigraphic flow, in one locality at the extreme western tip of the Santa Ynez Fault system, approaches the thickness of the Monterey Formation (700 m in this locality). However, in their case study, basinal fluids are predominantly focused into the fault zone over external fluids because the distance of formation-parallel fluid flow is found to exceed the distance of cross-stratigraphic flow.

6.2. Relative scale of fluid–rock ratios as deduced from stable isotopes

The observed range in C and O stable isotope fractionations observed in carbonates from host limestones, their veins, and deformation zones results from increasing fluid infiltration. It can thus give information on the relative importance of fluid infiltration, and the corresponding integrated fluid–rock ratios, in the different pathways followed by fluid flows before, during, and after faulting. A relative scale of fluid–rock ratios can therefore be derived. It integrates the distance from the main fluid pathway (the fault core) and the nature of the pathways: deformation zones, veins, or host rocks. Deformation zones show lower C and O isotopic ratios than veins, and veins show lower isotopic ratios than their host rocks (Fig. 3). Thus, the C–O isotopes indicate increasing fluid–rock ratios from host rocks to veins, and from veins to deformation zones. At a large scale, host rocks show lower C and O isotopic ratios toward the fault core (Fig. 2). This indicates increasing fluid–rock ratios in host limestones toward the fault core. This is consistent with the structural observations that the number of deformation zones and the spatial density of veins increase toward the fault core. At a local scale, host rocks show lower C–O isotope ratios near deformation zones and in densely veined zones (Fig. 2).

The fact that veins show a wide range of isotope compositions intermediate between their host rock and deformation zone (Fig. 3) suggests that unless fluid–rock ratios are very high, the isotope composition of veins does not represent the original composition of the fluid because of extensive interactions with host rocks before the vein can be formed. Deformation zones are a mixture of reworked host material and precipitated secondary minerals that show multiple cross-cutting veins. These structural observations and the relative high fluid–rock ratios observed in deformation zones, compared to veins, indicate that deformations zones are infiltrated more than once, whereas veins rather represent single shots of fluids, except in the rare cases of wide multilayered veins observed in this work, corresponding to the crack seal mechanism (Ramsay, 1980).

Information gained from trace element geochemistry is consistent with the stable isotope results. When applied to the measured trace element patterns (see Table 5), the relative scale of integrated fluid–rock ratios gives consistent results with the observed absolute concentrations as well as the relative enrichments or depletions seen in REE and other trace elements for host rocks or veins and deformation zones, respectively (Figs. 5–7). Hence, the increasing REE depletion (respectively, enrichment) observed in veins and deformation zones (respectively, host rocks) toward the fault core (Figs. 6 and 7) goes with increasing integrated fluid–rock ratios.

6.3. Fluid trace elements are scavenged by host rocks

With increasing fluid–rock ratios, the trace elements are enriched in host limestones and depleted in veins and deformation zones (Figs. 6 and 7 and Table 5). This contrasted behavior implies that the fluids, which precipitated carbonates in veins and in deformation zones, had their trace elements scavenged by the host rocks. Passive trace element enrichment in host rock due to deformation, dissolution, and expulsion of the soluble species driven by pressure solution and volume reduction accounts for 40% (for REE) and cannot explain most of the observed enrichment

Table 5
Classification of samples with increasing fluid–rock ratios based on stable isotopes and REE

Sample	LP19 H	LP14 H	LP9 H	LP19 V	LP19 M	LP9 V	LP14 VM
Sample type	Host	Host	Host	Vein	Fault plane	Vein	Fault plane
Distance from fault core (m)	500	58	13	500	500	13	58
$\delta^{13}C$ (PDB)[a]	5.26	0.47	−0.66	−3.08	−4.32	−3.78	−4.14
$\delta^{18}O$ (SMOW)[a]	27.16	24.44	25.89	21.56	18.32	20.31	16.17
Rank in REE concentrations[b]	3	2	1	4	6	5	7
Rank in enrichment/depletion in REE[c]	1	2	3	4	5	6	7

[a] Data from Table 1.
[b] Data from Table 2.
[c] From Figs. 6 and 7, enrichment in host rocks, depletion in veins, and fault planes.

(up to a mean value of 700% for REE; see Fig. 6). Element fractionation is not expected to occur for crystal chemistry reasons since the leached and the precipitating crystals are essentially of similar nature (Ca–Mg carbonates). However, the newly precipitated carbonate crystals might lack impurities present in the host sedimentary carbonates, which might prevent the REE to coprecipitate in the veins and deformation zones. Alternatively, the host rocks may offer efficient sites for REE complexation in the form of organic matter or clays.

Aqueous fluid transport is involved in the present case and it has been shown that chemical fractionation of geochemical pairs with similar ionic radii and charge such as Y and Ho or Zr and Hf may occur if these elements are complexed with aqueous ligands (Bau, 1996). Unfortunately, the Zr–Hf geochemical pair cannot be used in the present study because Hf is often below detection limits for veins and deformation zones (see Table 2). However, Nb and Ta share also similar charge and ionic radius for a given coordination and may therefore be used instead. The utilization of the Nb–Ta geochemical pair has been hindered until recently because these elements used to be determined by different techniques that prevented the determination of accurate and precise Nb/Ta ratios (Green, 1995). However, the advent of ICP-MS made it possible to analyze these two elements simultaneously down to the low ppb level (e.g., Poitrasson et al., 1993). The Nb/Ta and Y/Ho ratios found in rocks for which chemical fractionation affects mostly elements with different charge and ionic radius (e.g., magmatic crystal fractionation) are defined as an "extended CHARAC" field (CHArge and RAdius Controlled trace element behavior) in Fig. 9, by extrapolation of the work of Bau (1996) for Y–Ho, to the survey of Green (1995) for Nb–Ta in various terrestrial reservoirs. The first observation is that all the host rock sample series (LP9 H, LP14 H, LP19 H, and P1–P6) plot out of the "extended CHARAC" field (Fig. 9), as expected for limestones formed by aqueous precipitation of ions in seawater. Secondly, all the veins and deformation zones plot even further away than the host rocks from the field where the element behavior is only controlled by charge and ionic radius. This suggests that complexation of trace elements by aqueous ligands occurred during permeation of the host rocks by the fault fluids. These ligands may be responsible for the scavenging of the fluid trace elements by the host rocks, resulting in the observed enrichment (Fig. 6). Lastly, the three host rocks–veins or host rocks–deformation zones pairs

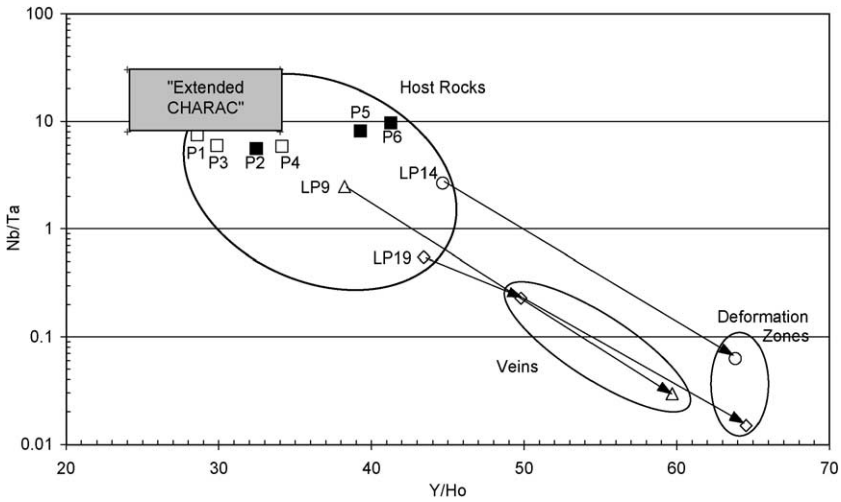

Fig. 9. Plot of the Nb–Ta ratios vs. Y–Ho ratios for all the analyzed samples, subdivided into host rocks, veins, and deformation zones. Data are from Tables 2 and 3. The variously deformed host rocks from the P sample series are depicted with open squares for the most deformed samples and solid squares for the least deformed ones. Other samples as indicated on the figure. The "extended CHARAC" field is defined after Bau (1996) and Green (1995) (see text). Trace element fractionation induced by external fluid infiltration is much larger (see the fields for veins and deformation zones) compared to those induced by deformation (see the field for host rocks).

define vectors having the same direction in the Nb/Ta vs. Y/Ho diagram (Fig. 9), suggesting that similar ligands were operating in all cases. Specifically, the organic matter contained by the Monterey limestones could be responsible for most of the complexation. The magnitude of the filtration is correlated with the relative scale of fluid–rock ratios as given by the stable isotope systematics.

A few trace elements (Ba, Pb, and to some extent Sr) do not follow the general enrichment trend observed in host rocks (Fig. 6) with decreasing distance toward the fault core over 500 m and increasing fluid–rock ratios. Unlike other trace elements, these three elements are not expected to be involved in a passive scavenging. They are essentially divalent in geological environments and can substitute easily in the carbonate cationic site. Accordingly, they show among all the analyzed trace elements the highest concentrations measured in most samples (Table 2). Hence, whereas these rather soluble elements will mostly be leached out of the carbonate crystallographic sites during the fluid–rock events, the other trace elements, initially less abundant and also less mobile in aqueous solutions, will be preferentially concentrated in the percolated rocks, possibly by a combination of pressure–solution and complexation processes. The same behavior for Ba and Sr is seen in the variously deformed host rocks (sample series P1–P6; Fig. 8), but a reverse behavior for Pb is seen, yet unexplained.

6.4. Fluid pathways

Two main types of fluid pathways, one pervasive in the host rocks and the other channeled in veins and deformation zones, are here evidenced. The above structural and geochemical observations show that faults maintain a high permeability during, and at least temporarily after, an earthquake due to veins and deformation zones that are progressively sealed. However, fluid flow is not only channeled in veins and deformations zones. The extensive interactions between host rocks and the fluids that flow in veins and deformation zones, responsible for their isotope ratio and trace element concentration changes (Figs. 3, 6, and 7) and for the isotope shifts observed in host rocks toward the fault zones (Fig. 2), indicate that part of the fluid flow related to faults occurs pervasively in the host rocks, with increasing pervasive fluid infiltration toward the fault core. A pervasive fluid flow is also implied by the 30% volume decrease of the host rocks associated with deformation over tens of meters from the fault core.

Three hypotheses may be brought forward to explain why veins and deformation zones are increasingly depleted in REE while their host rocks are increasingly enriched as fluid–rock ratios increases toward the fault core.

(1) The REE may be present in the vein fluid and held back as incompatible elements when carbonate crystals form. In such case, the fluid would become enriched in REE as precipitation occurs, and the sinks for these extra REE would be the host rocks that subsequently scavenge them during pervasive flow. The existence of some unknown REE deposits in veins is not considered here. An important consequence of this hypothesis is that the fluid flows first (and mainly) within the veins and deformation zones, and subsequently (and to a lesser extent), the fluid flows pervasively within the host rocks. Fluids are in this hypothesis discharged from the fault via veins and deformation zones, then into the host rocks. This is the ‘‘focused fluid flow hypothesis’’.

(2) The host rocks scavenge the REE present in the fluid before it precipitates REE-depleted carbonate crystals in veins and deformation zones. This is the ‘‘pervasive fluid flow hypothesis’’ where the fluid flows first (and mainly) within the host rocks and is discharged to the veins and deformation zones. The source for the REE-enriched fluid is the leaching of the carbonate sequence, presumably in horizons poor in organic matter, which prevents local REE complexation.

(3) Fluid flow is channeled in veins and deformation zones, but the fluid wets the host rocks and has its REE scavenged. This is the ‘‘mixed focused–pervasive fluid flow hypothesis’’ where the fluid mainly flows within veins and deformation zones, but the REE fluid composition is controlled simultaneously by filtration in the host rocks where part of the fluid flows pervasively. This leads to the formation of REE-depleted veins and deformation zones, and simultaneously of REE-enriched host rocks, with depletion and enrichment increasing as fluid–rock ratios increase. The Ce-negative anomaly inherited from the seawater carbonate host rocks is preserved in the vein and deformation zone carbonate fillings.

The present work brings evidence for the "mixed focused–pervasive fluid flow hypothesis". The other hypotheses are not to be completely ruled out, but they do not fully characterize the fluid–rock system. The "focused fluid flow hypothesis" where fluids are discharged from the fault via veins and deformation zones into the host rocks is true at the first order (kilometer scale). This is the mechanism by which exotic fluids are supplied (from depth) to the system. However, this mechanism is not likely to explain the REE behavior observed at the local scale because it requires an improbable series of events. (i) The carbonate crystals that precipitate in veins and deformation zones are not able to incorporate REE when they form so that the fluid remaining after carbonate precipitation is enriched in REE. This mechanism fails to account for the Ce anomaly indicating that the REE contents of the fluid flowing into the faulted Monterey Formation are controlled by the carbonate sequence itself. (ii) As the fracture is sealed by carbonate precipitation, the fluid flows in the host rock, and not in some other fracture that opens farther. (iii) The host rock absorbs all the fluid and its high REE contents. The "pervasive fluid flow hypothesis" where the fluid is discharged from the host rocks to the fault accounts for some host rock volume reduction and lateral fluid migration into fault zones. Also, such a mechanism must exist at least at the source points of exotic fluids that are focused into other faulted formations. However, the REE enrichment observed in host rocks cannot only result from pressure solution and decrease in the rock volume. Furthermore, the REE enrichment observed in host rocks goes with increasing exotic fluid infiltration. Thus, the host rock REE enrichment must result from percolation of the carbonate host rocks by external fluids flowing in veins and deformation zones.

An estimation of the relative volumes of host rocks, veins, and deformation zones is lacking to calculate at which scales the REE partitioning can be considered to occur in a closed or an open system. This would lead to an estimation of the scales at which the different components of the fluid system operate, and a quantification of the fluid–rock ratios. Nevertheless, our study shows that the external fluid flow operates at the order of kilometers, and the internal fluid flow at the order of meters to tens of meters. The relative concentration effects on REE of the fluids focused from depth into veins and deformation zones compared to those flowing pervasively from host rocks may be estimated from the REE enrichment factors, respectively, a total factor of 8 (+700%) resulting both from external fluid infiltration and internal fluid production, and a specific factor of 1.4 (+40%) resulting from internal fluid production only. If the two phenomena are superimposed, this would lead to a specific REE enrichment factor of 5.7 for external fluid infiltration and a specific REE enrichment factor of 1.4 for internal fluid production. In this case, fluid infiltration would be four times more efficient than deformation for REE concentration. However, some reverse chemical changes, yet unexplained, observed in the two sample sets used in this study to document different aspects of fluid–rock interactions at various scales in the faulted carbonate sequence cast some doubts on whether the REE enrichment factors can be combined.

7. Conclusions

Numerous samples from the Little Pine Fault, a part of the San Andreas Fault system, provided a well-documented insight into the detailed chemical and isotopic evolution of host rocks undergoing deformation from the scale of centimeters to hundreds of meters, and of host rocks, veins, and deformation zones as infiltration increases over tens to hundreds of meters toward the fault core. For the first time to our knowledge, this study has combined C–O isotope data with a comprehensive trace element data set to examine the geometry of fluid flow within a significant fault system hosted by a carbonate sequence.

Rocks exposed along the Little Pine Fault recorded fluid–rock interactions related to faulting. The fault maintains a high permeability during and, at least temporarily, after earthquakes due to veins and deformation zones that are progressively sealed. The fluids that flow in sufficient quantities and with contrasted-enough chemical and isotopic compositions to leave a detectable signature in host rocks, veins, and deformation zones are H_2O–CO_2 mixtures. Fluid infiltration increases toward fault core over 500 m. Fluid–rock ratios increase from host rocks, veins, and deformation zones. The fault zone at Little Pine is an open system. Two fluid sources, one internal and

the other external, are evidenced from the stable isotope and trace element constraints. The external fluid is inferred to come principally from metamorphism of the Franciscan formation underneath. The internal (local) fluid is provided by the 30% volume reduction of the host limestones resulting from deformation and pressure solution, and is expelled toward dilatant structures: the veins and the deformation zones.

The C–O isotope compositions are closely related in host rocks whereas they are variously correlated in veins and deformation zones. The C and O isotope fractionations can be large in fault zone host rocks compared to unaltered ones, and in veins or deformation zones compared to their host rocks. Stable isotope geochemistry is used to establish a relative scale of integrated fluid–rock ratios. From highest to lowest delta values, thus from least to most infiltrated, are the host rocks, the vein fillings, and the deformation zone fillings, respectively. Infiltration increases toward fault core. With increasing fluid–rock ratios, the trace elements are enriched in host limestones and depleted in veins and deformation zones. This contrasted behavior implies that the fluids that precipitated carbonates in veins and in deformation zones had their trace elements scavenged by the host rocks, probably through organic matter complexation. A total REE enrichment factor of 8 (+700%) resulting both from external fluid infiltration and also possibly from internal fluid production, and a specific REE enrichment factor of 1.4 (+40%) resulting from internal fluid production, have been calculated. Stable isotopes and trace elements geochemistries show consistent evidence for structurally controlled fluid flow during faulting. The coherent behavior of trace elements and stable isotopes is illustrated in Fig. 10, the increases in the Y/Ho ratios being correlated with the decrease in $\delta^{13}C$ or $\delta^{18}O$. The C–O isotope ratios are especially sensitive to external fluid infiltrations and high fluid–rock ratios, whereas elemental complexation is especially illustrated by large fractionation of Y/Ho and Nb/Ta geochemical pairs. The $\delta^{13}C$ or $\delta^{18}O$ and the Y/Ho or Nb/Ta ratios are equally good tools to document fluid infiltrations because they are independent and sensitive, and they offer a good resolution.

Our observations from the millimeter to the kilometer scale call for the partitioning of fluid sources and pathways, and for a mixed focused–pervasive fluid flow mechanism. The fluid mainly flows within veins and deformation zones and, simultaneously, within at least 10 cm from these channels, part of

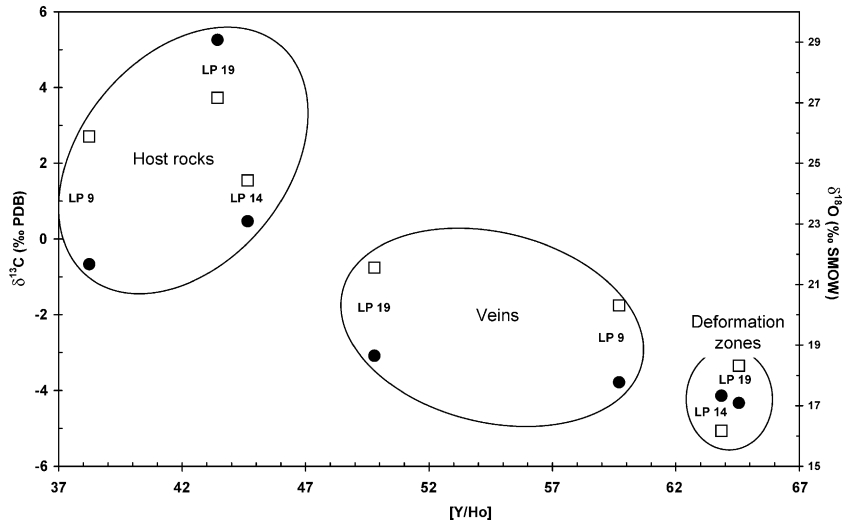

Fig. 10. Plot of the Y–Ho ratio vs. $\delta^{13}C$ (black circles) and $\delta^{18}O$ (white squares) for all the analyzed samples, subdivided in host rocks, veins, and deformation zones. Data are from Table 2. Samples as indicated on the figure. Stable isotopes and trace element fractionations in host rocks, veins, and deformations induced by external fluid infiltration show consistent results.

the fluid flows pervasively in the host rock, which controls the fluid composition. Scavenging of the fluid REE by host rocks, presumably through organic matter complexation, is responsible for the formation of REE-depleted veins and deformation zones. The Ce-negative anomaly inherited from the seawater carbonate host rocks is preserved in the vein and deformation zone carbonate fillings. Increasing external fluid infiltration in veins and deformation zones goes with increasing pervasive fluid flow in the adjacent host rocks. Fluid flow is not only restricted to veins or deformation zones, which are transient bypass. An important part of fluid flow takes place in host rocks near fault zones, possibly even when fractures are closed or sealed. Hence, the nature of the lithologies hosting fault zones, and their potential to react with the fluid and to rupture at given fluid pressure, must be considered in order to take into account the role of fluids in the seismic cycle. The important role of host rocks in controlling faulting has also been suggested from electromagnetic imaging of the SAF (Unsworth et al., 1999). The distance of hundreds of meters observed here for the onset of fault-related fluid infiltration is consistent with what is observed in the electromagnetic imaging.

Acknowledgements

This work benefited from stimulating discussions and presentations at the Euresco 2000 conference "Geochemistry of Crustal Fluids", particularly from Susan Brantley, Art White, and Bjørn Jamtveit. Support by the Euresco Program to attend the meeting in Granada is appreciated. This work was partly supported by the DOE under contract "San Andreas Fault Fluid Chemistry" to B. Mack Kennedy. Éric Pili was sponsored by the French Ministry of Foreign Affairs "Bourse Lavoisier" 1997 Postdoctoral Award. Éric Pili thanks Mack Kennedy, Mark Conrad, and Don DePaolo for hosting him during his postdoctoral research, for access to the stable isotope laboratory facilities, and for stimulating discussions. Additional research support from the France-Berkeley Fund (1998 Award) has been greatly appreciated. Thanks go to S.F. Cox and Z.D. Sharp for constructive journal reviews, and to S.R. Gislason for editorial handling.**[EO]**

References

Bau, M., 1996. Controls on the fractionation of isovalent trace elements in magmatic and aqueous systems: evidence from Y/Ho, Zr/Hf, and lanthanide tetrad effect. Contrib. Mineral. Petrol. 123, 323–333.

Boullier, A.-M., Robert, F., 1992. Palaeoseismic events recorded in Archaean gold–quartz vein networks, Val d'Or, Abitibi, Quebec, Canada. J. Struct. Geol. 14, 161–179.

Carignan, J., Hild, P., Mevelle, G., Morel, J., Yeghicheyan, D., 2001. Routine analyses of trace elements in geological samples using flow injection and low pressure on-line liquid chromatography coupled to ICP-MS: a study of geochemical reference materials BR, DR-N, UB-N, AN-G and GH. Geostand. Newsl. 25, 187–198.

Dibblee, T.W., 1966. Geology of the Central Santa Ynez Mountains, Santa Barbara County, California. California Division of Mines and Geology Bulletin 186. California Division of Mines and Geology, San Francisco, 99 pp.

Eichhubl, P., Boles, J.R., 2000. Focused fluid flow along faults in the Monterey Formation, coastal California. Geol. Soc. Am. Bull. 112 (11), 1667–1679.

Fleet, A.J., 1984. Aqueous and sedimentary geochemistry of the rare earth elements. In: Henderson, P. (Ed.), Rare Earth Element Geochemistry. Elsevier, Amsterdam, pp. 343–373.

Gratier, J.P., 1983. Estimation of volume change by comparing chemical analyses in heterogeneously deformed rocks. J. Struct. Geol. 5, 329–339.

Gratier, J.P., Chen, T., Hellman, R., 1993. Pressure solution as a mechanism for crack sealing around faults. In: Hickman, S., Sibson, R., Bruhn, R. (Eds.), Proceeding of the Workshop LXIII "The Mechanical Involvement of Fluids in Faulting". U.S Geological Survey, Menlo Park, Ca, pp. 279–300.

Gratier, J.-P., Favreau, P., Renard, F., 2001. Modeling fluid transfer along Californian faults when integrating pressure solution crack-sealing and compaction processes. J. Geophys. Res. submitted for publication.

Green, T.H., 1995. Significance of Nb/Ta as an indicator of geochemical processes in the crust–mantle system. Chem. Geol. 120, 347–359.

Hickman, S., Sibson, R., Bruhn, R., 1995. Introduction to special section: mechanical involvement of fluids in faulting. J. Geophys. Res. 100 (B7), 12831–12840.

Irwin, W.P., Barnes, I., 1975. Effect of geologic structure and metamorphic fluids on seismic behavior of San Andreas Fault system in central and northern California. Geology 3, 131–143.

Jamtveit, B., Austrheim, H., Malthe-Sorenssen, A., 2000. Accelerated hydration of the Earth's deep crust induced by stress perturbations. Nature 408, 75–78 (2 November).

Jennings, C.W., 1994. Fault Activity Map of California and Adjacent Areas with Location and Ages of Recent Volcanic Eruptions. California Division of Mines and Geology, Sacramento.

Lachenbruch, A.H., Sass, J.H., 1980. Heat flow and energetics of the San Andreas Fault zone. J. Geophys. Res. 85 (B11), 6185–6223.

Li, Y.-G., Vidale, J.E., Aki, K., Xu, F., Burdette, T., 1998. Evidence of shallow fault zone strengthening after the 1992

M7.5 Landers, California, earthquake. Science 279, 217–219 (9 January).
Liu, Y.G., Miah, M.R.U., Schmitt, R.A., 1988. Cerium; a chemical tracer for paleo-oceanic redox conditions. Geochim. Cosmochim. Acta 52, 1361–1371.
Magaritz, M., Taylor Jr., H.P. 1976. Oxygen, hydrogen and carbon isotope studies of the Franciscan Formation, Coast Ranges, California. Geochim. Cosmochim. Acta 40, 215–234.
McCrea, J.M., 1950. On the isotopic chemistry of carbonates and a paleotemperature scale. J. Chem. Phys. 18, 849–857.
Nakamura, N., 1974. Determination of REE, Ba, Fe, Mg, Na and K in carbonaceous and ordinary chondrites. Geochim. Cosmochim. Acta 38, 757–775.
O'Neil, J.R., Hanks, T., 1980. Geochemical evidence for water–rock interaction along the San Andreas and Garlock faults of California. J. Geophys. Res. 85 (11), 6286–6292.
Pili, É., Kennedy, B.M., Conrad, M.S., Gratier, J.-P., 1998. Isotope constraints on the involvement of fluids in the San Andreas Fault. EOS Trans. AGU 79 (17) Spring Meet. Suppl. S229, April 28.
Poitrasson, F., Pin, C., Telouk, P., Imbert, J.L., 1993. Assessment of a simple method for the determination of Nb and Ta at the sub-mg/g level in silicate rocks by ICP-MS. Geostand. Newsl. 17, 209–215.
Poitrasson, F., Pin, C., Duthou, J.L., 1995. Hydrothermal remobilization of rare earth elements and its effects on Nd isotopes in rhyolite and granite. Earth Planet. Sci. Lett. 130, 1–11.
Poitrasson, F., Paquette, J.L., Montel, J.M., Pin, C., Duthou, J.L., 1998. Importance of late-magmatic and hydrothermal fluids on the Sm–Nd isotope mineral systematics of hypersolvus granites. Chem. Geol. 146, 187–203.
Ramsay, J.G., 1980. The crack-seal mechanism of rock deformation. Nature 284, 135–139 (13 March).
Rice, J.R., 1992. Fault stress, pore pressure distribution, and the weakness of the San Andreas Fault. In: Evans, B., Wong, T.-F. (Eds.), Fault Mechanics and Transport Properties of Rocks. International Geophysics Series. Academic Press, London, pp. 475–503.
Robert, F., Boullier, A.-M., Firdaous, K., 1995. Gold–quartz veins in metamorphic terranes and their bearing on the role of fluids in faulting. J. Geophys. Res. 100 (B7), 12861–12879.
Scholz, C.H., 1989. The Mechanics of Earthquakes and Faulting Cambridge Univ. Press, Cambridge, UK, 439 pp.
Sibson, R.H., 1992. Fault-valve behavior and the hydrostatic–lithostatic fluid pressure interface. Earth Sci. Rev. 32, 141–144.
Sibson, R.H., 1994. Crustal stress, faulting and fluid flow. In: Parnell, J. (Ed.), Geofluids: Origin, Migration and Evolution of Fluids in Sedimentary Basins. The Geological Society, London, pp. 69–84.
Unsworth, M.J., Egbert, G.D., Booker, J.R., 1999. High-resolution electromagnetic imaging of the San Andreas Fault in central California. J. Geophys. Res. 104 (B1), 1131–1150.
Wallace, R.E. (Ed.), 1990. The San Andreas Fault System, California, 1515. US Government Printing Office, Washington 283 pp.
Winter, B.L., Knauth, L.P., 1992. Stable isotope geochemistry of carbonate fracture fills in the Monterey Formation, California. J. Sediment. Petrol. 62 (2), 208–219.